

# Heterogeneity meets disorder: anomalous wave transport in telescopic metamaterials

Paolo Celli\* and Stefano Gonella†

*Department of Civil, Environmental, and Geo- Engineering,  
University of Minnesota, Minneapolis, MN 55455, USA*

\*pcelli@umn.edu, †sgonella@umn.edu

December 14, 2024

In this work, we report on a family of subwavelength wave manipulation effects experimentally observed in thin elastic metamaterial sheets endowed with heterogeneous populations of tunable telescopic resonators. We first document the achievement of extremely broadband mechanical filtering, which results from the interplay between the spatial disorder and the functional heterogeneity of the population of resonators. Specifically, we illustrate how randomized spatial arrangements consistently outperform their functionally graded counterparts in terms of maximum achievable bandgap width. By fully leveraging the agility by which we can turn on and off localized pockets of heterogeneity, we then proceed to realize a variety of waveguides obtained by opening paths of frequency-upshifted resonators within an otherwise uniform architecture. This effort results in a first set of preliminary experimental observations of subwavelength confinement in the context of elastodynamics. Our investigation shows that the design space of mechanical metamaterials can be stretched beyond the limits imposed by order and homogeneity, thus highlighting the engineering significance of the emerging concepts of organized disorder and design modularity.

## Significance statement

The dominant approach in the design of metamaterials for vibration and wave control revolves around ordered arrangements of identical resonators. In this work, we unveil through experiments a family of unique wave manipulation effects that challenge this paradigm and are directly enabled by the interplay between the mechanical heterogeneity and the spatial disorder of the resonators population. The experiments are carried out using reconfigurable specimens with telescopic pillars whose resonant characteristics can be agilely and intuitively tuned through simple manual operations. We demonstrate that spatial disorder can be leveraged to enhance the already remarkable broadband filtering capabilities of so-called rainbow materials. We also provide a first preliminary evidence of subwavelength wave transport phenomena in elastic waveguides involving frequency up-shifted resonators.

## Introduction

Due to their peculiar mesoscale architectures, metamaterials are capable of attenuating [1], anomalously refracting [2], focusing [3], cloaking [4], imaging [5], trapping [6] and guiding [7] waves in the *subwavelength* regime—when the wavelengths are much larger than the characteristic microstructural length scales of the medium. Some of these effects, like subwavelength waveguiding and rainbow trapping, require the coexistence of *heterogeneous* populations of resonators, i.e., resonators with different resonant characteristics. For example, subwavelength waveguiding (where the width of the waveguide is the defining length scale of the problem) has been achieved by opening paths of defects in a

periodic medium with resonators, and by placing up-shifted resonators along the defected paths [7–10]. Similarly, rainbow trapping requires arrays of resonators with functionally graded characteristics, where each resonator distills a selected frequency from a broadband input signal [6, 11–16].

Inspired by recent developments in electromagnetics and acoustics, we set forth to investigate subwavelength phenomena in the realm of elastodynamics, where peculiar effects result from the interplay between the heterogeneity of the resonators, their spatial organization, and the mechanical coupling between them. Our wave-carrying medium of choice is a stubbed plate, i.e., a thin sheet with pillar-like resonators [17–25]. We intend to show that the already broadband wave attenuation achievable with functionally-graded arrangements of pillars can be systematically improved by spatially randomizing the pillar configuration. In a second set of experiments, we deploy sets of frequency up-shifted resonators in selected subregions of the domain, with the objective of eliciting a family of subwavelength waveguiding phenomena whose peculiar characteristics are germane to the realm of elastodynamics.

In order to achieve the versatility required to test multiple architectures within a single reconfigurable specimen, we assemble a modular stubbed plate with *telescopic* resonators. The desired modularity [26–28] is achieved using a flexible fabrication framework, inspired by our previous experimental work [25], which involves the arrangement of arrays of LEGO<sup>®</sup> bricks on a thin baseplate. Here, as shown in Fig. 1, additional flexibility is granted by the fact that each resonator consists of a rod and a conical brick, and can be tuned by sliding the brick up and down, which

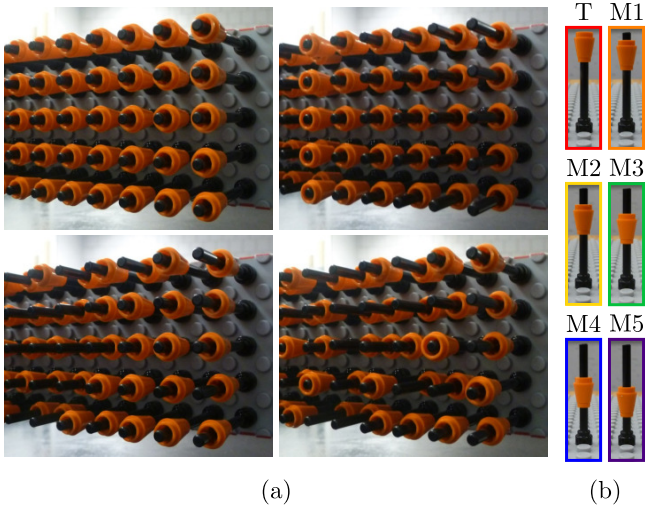


FIGURE 1: (a) Detail of selected pillar configurations: one uniform, one graded and two realizations of randomized resonators arrangements. (b) Families of resonators (from T to M5) available from a single telescopic pillar element by sliding the conical brick down the rod by discrete increments.

effectively alters its inertial characteristics and its natural frequencies. This “manual” tuning strategy is conceptually similar to those discussed by other authors for Bragg bandgap tunability [29–31].

## Setup and response of uniform architectures

Our experimental setup is schematically illustrated in Fig. 2. The specimen (a detail of which is shown in Fig. 1a)

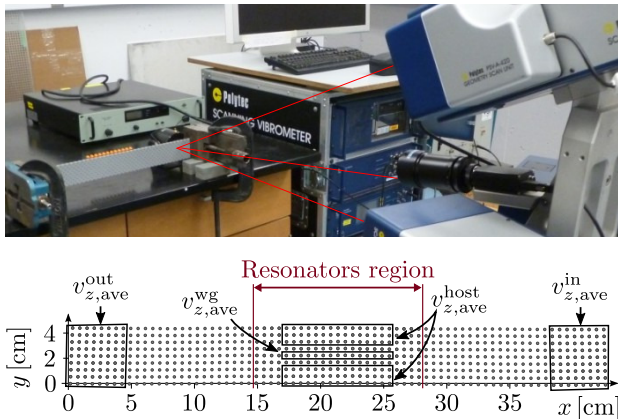


FIGURE 2: Experimental setup (top) and measurement grid (bottom, where the boxes encircle groups of points used to calculate specific quantities mentioned in the text).

consists of a long strip cut out from a baseplate, and features an array of telescopic resonators arranged in a square lattice. The resonators can assume one of the six quantized inertial configurations shown in Fig. 1b, obtained by sliding the conical brick down the rod by discrete incre-

ments (3.25 mm). Each configuration is color-coded to visually illustrate how the resonators are spatially arranged in each experiment. The metamaterial plates are probed with a pseudorandom waveform to analyze standing wave patterns over a broad spectrum of frequencies, and their out-of-plane response is recorded with a 3D Scanning Laser Doppler Vibrometer (3D-SLDV). More details on the setup are discussed in the *Materials and Methods* and *Supplementary Material* sections.

The frequency responses of six arrangements of 60 uniformly-tuned resonators, used as baseline throughout our experiments, are shown in Fig. 3. Each line is a trans-

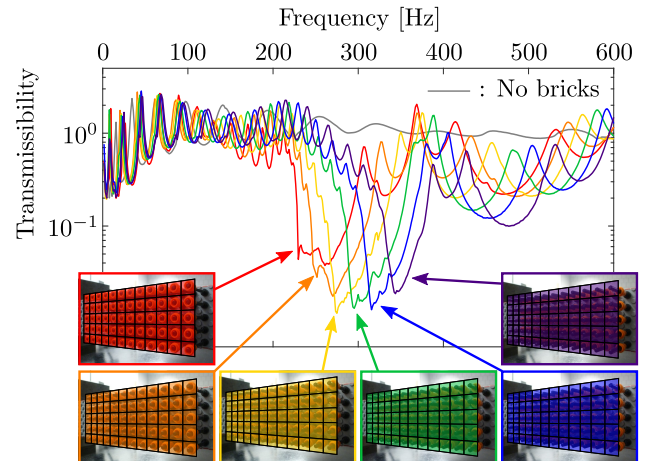


FIGURE 3: Comparison between the transmissibilities of configurations featuring uniform arrangements of  $5 \times 12$  pillars. The inserts represent the configurations corresponding to each transmissibility line. For illustration purposes, we superimpose to the pillars a grid of colored squares according to the color code introduced in Fig. 1b.

missibility curve, obtained (for the configuration shown in the corresponding insert) by plotting  $v_{z,ave}^{out}/v_{z,ave}^{in}$ , where  $v_{z,ave}^{in}$  and  $v_{z,ave}^{out}$  are the average velocity measured at points near and far from the source, respectively (see Fig. 2 for a visual map of the measurements involved in all calculations). These results illustrate that each configuration features a locally resonant bandgap (here we qualify as bandgaps regions where the transmissibility is smaller than 0.2), and that the resonators are tuned as to display overlapping bandgaps. The onsets of the bandgaps shift with remarkable consistency towards higher frequencies as the inertia of the resonators is decreased.

## Disorder-enhanced bandgap widening

Locally resonant bandgaps are narrow in nature. This limitation has inspired numerous widening strategies, among which we recall trampoline effects [32], rainbow trapping [12], bandgap adjoining [33, 34], and disorder-based methods involving Anderson localization effects [35, 36]. Here, we specifically investigate the dependence of the bandgap width upon the order attributes (or lack thereof)

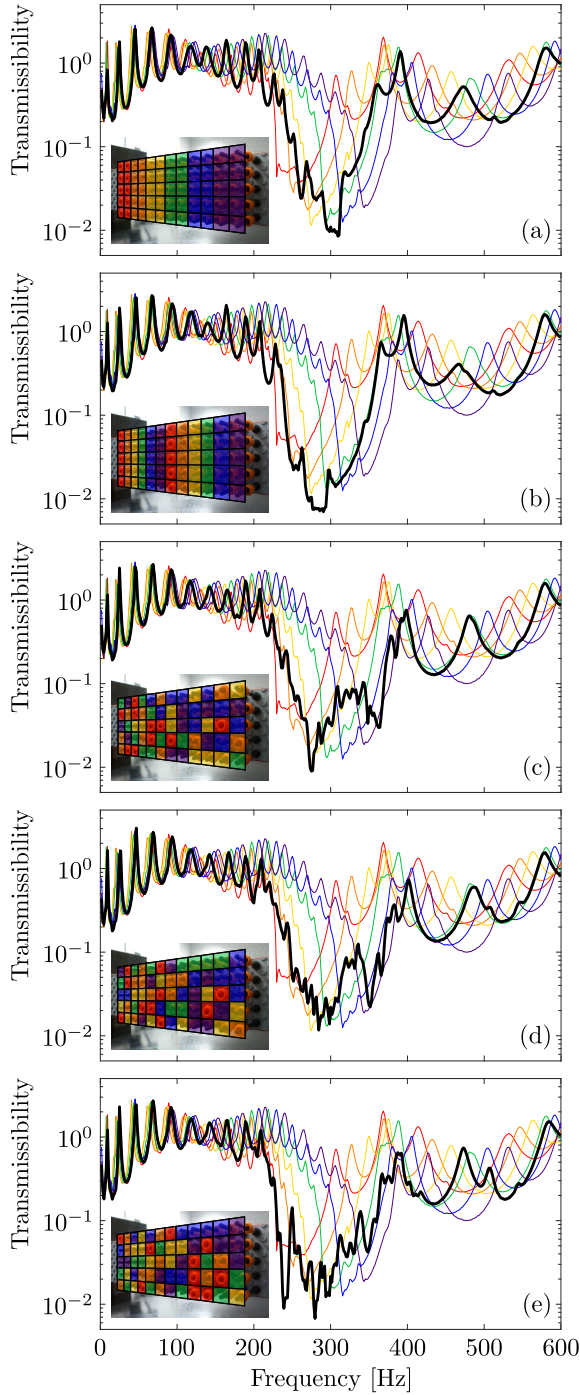


FIGURE 4: Influence of the spatial arrangement of heterogeneously tuned resonators on wave attenuation. The resonators are programmed according to the indicated color schemes; in all cases, the resonators are divided in six groups of ten units each, implementing the six pillar configurations shown in Fig. 1b, so that the volume fraction of each type is preserved from case to case. (a), (b) Transmissibilities for functionally graded and (c), (d), (e) spatially randomized configurations, marked by thick black lines; thin color-coded lines refer to uniformly tuned monochromatic configurations.

of heterogeneous populations of resonators. To this end, we compare the performance of three classes of configurations: uniform resonators, graded arrangements of heterogeneous resonators, and random populations of heterogeneous resonators. The transmissibilities of a few selected cases are shown in Fig. 4. In each subfigure, the thick black line represents the transmissibility for the arrangement shown in the corresponding insert; all the architectures feature 10 resonators of each kind—T, M1, M2, M3, M4, M5 following the color coding introduced in Fig. 1b. The thin colored lines are the transmissibilities for the homogeneous configurations depicted in Fig. 3, shown for reference.

The results for two graded architectures with different gradient periodicity are compared in Figs. 4a-b and clearly highlight a widening of the bandgap with respect to their monochromatic counterparts. In both depicted cases, the total bandgap spans the frequency interval encompassing the individual gaps of three monochromatic configurations. This result is in line with the rainbow trapping paradigm [12–14]. Interestingly, we also notice that the maximum attenuation (dip in the transmissibility curve) achieved with graded rainbow architectures is larger than that observed for any of the uniform cases, despite the fact that rainbow configurations feature a smaller number of resonators for each type. Further comparing the performance of the two graded scenarios, we observe that the configuration in Fig. 4b produces a wider and deeper gap than the one in Fig. 4a, which suggests that the performance of graded architectures is influenced by the period of the spatial arrangement. The transmissibilities for three representative *disordered* arrangements are shown in Figs. 4c-e. It is important to note that all the randomized configurations involve the same six classes of resonators, and the same volume fraction of resonators for each class, of the graded cases. The most distinctive morphological difference brought about by randomization is a “jagged” profile of the bandgap. More importantly, the bandgaps are consistently wider than their counterparts observed for graded configurations—stretching here over the frequency regions spanned by four (or even five) individual bandgaps. As shown in the *Supplementary Material*, the latter result is observed systematically across a wide pool of tested random configurations.

A more detailed account of the observed bandgap widening is provided in Fig. 5. In Fig. 5a, we superimpose the transmissibilities of three systems: a uniform arrangement of M3 resonators, the graded architecture shown in Fig. 4b and the random one of Fig. 4e. Clearly, adding disorder to heterogeneity increases the bandgap width: if, for instance, we consider the two test frequencies 239 Hz and 359 Hz marked in Fig. 5a, at which both the homogeneous and the ordered heterogeneous system are in transmission mode, we see that they fall well within the bandgap for the random configuration. In Fig. 5b, for the same three configurations, we plot the (normalized) response sampled along the mid line of the strip at three characteristic fre-

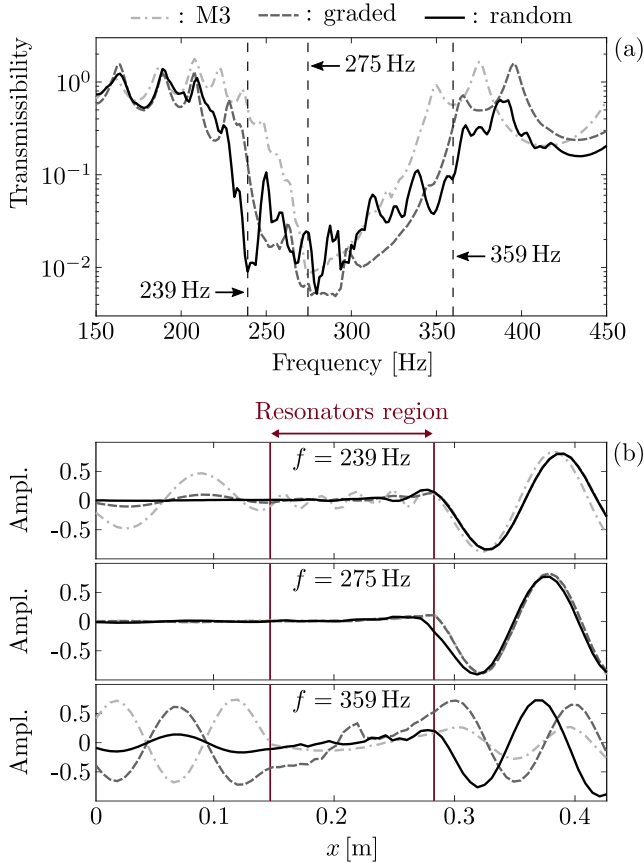


FIGURE 5: (a) Comparison between the bandgap performance of uniform, graded and random architectures. (b) Normalized mode shapes measured along the mid-span of the plate, for the three architectures considered in (a) and at three characteristic frequencies. Note that the excitation is applied at the right end of the domain.

quencies. We see that, while at 275 Hz all the configurations effectively attenuate waves, at 239 Hz and 359 Hz the random architecture vastly outperforms the others in terms of filtering.

The disorder-enabled widening of the bandgap and the alteration of its shape are consistent with the observations reported for a number of systems in which the widening and morphological evolutions of “transmission gaps” have been linked to Anderson localization effects [35–38]. Based on this analogy, we can conjecture that localization mechanisms are also likely to play an important role in our experiments. However the extent to which the interpretation obtained for other acoustic systems can be seamlessly transferred to the peculiar problem of thin elastodynamic sheets with pillar-like resonators remains an open question and will require a separate theoretical treatment. Here we limit ourselves to note a few distinctive features of our mechanical system. In contrast with the cases studied by Thorp et al. [35] and Sainidou et al. [36], the widening effect is here observed in the context of hybridization bandgaps and therefore occurs in the subwavelength regime. Moreover, it

is manifestly a result of adding spatial randomization to an already mechanically heterogeneous system, while in previous works the two concepts of randomness and heterogeneity intrinsically overlapped. Finally, here the resonators are not coupled directly, as in other disordered systems such as networks of sintered spheres [39], but rather weakly through the elastic substrate. The strength of this coupling and the possible mismatch between the phononic characteristics of the resonators and those of the substrate most likely control the manifestation of the observed effects.

## Subwavelength waveguiding

It has been demonstrated by Lemoult et al. that subwavelength waveguiding and confinement can be obtained in locally-resonant acoustic and electromagnetic metamaterials by introducing defects featuring up-shifted resonators [7]. The phenomenon can be explained invoking Fano-type interference mechanisms, whereby a resonator impinged upon by an incident wave stores energy and re-radiates it into the medium. If the frequency of the incoming wave is slightly larger than its resonance, incoming and re-radiated waves have opposite phase and destructively interfere, causing the opening of a subwavelength bandgap (which in fact begins at resonance and ends when the amplitude of the resonator spectrum tapers off). At frequencies right before resonance, on the other hand, incoming and re-radiated waves interact constructively. When we place an up-shifted resonator within a host medium in bandgap mode, waves tend to localize near the outlier due to the local availability of constructive interference—while destructive interferences bar them from propagating elsewhere. This results in waveguiding or confinement, depending on the arrangement of the resonators. This behavior, unlike that observed in systems with vacancy-like defects and empty waveguides [20, 25, 40, 41], extends to scenarios where the wavelength is significantly larger than the characteristic size of the defect (or the width of the waveguide). To date, only few theoretical studies have addressed subwavelength waveguiding in elastic media [42], and these phenomena still beg for experimental evidence.

In Fig. 6, we compare two configurations. The first features an empty waveguide in a M1 host lattice. The transmissibility is represented by the thick black line in Fig. 6a. The absence of additional transmission features inside the bandgap (with respect to the orange line, obtained for a uniform M1 architecture) suggests that the waveguide is too narrow to allow wave propagation at those frequencies. Similar conclusions can be reached from Fig. 6b, which shows the dispersion relation reconstructed from the steady-state data acquired at measurement points along the defected path. The plot, very similar to the dispersion relation for a uniform M1 architecture (see *Supplementary Material*), features two branches separated by a resonant bandgap. In Fig. 6c, we plot the ratio between the average velocity measured inside the waveguide ( $v_{z,\text{ave}}^{\text{wg}}$ ) and that measured inside the surrounding M1 region ( $v_{z,\text{ave}}^{\text{host}}$ ):

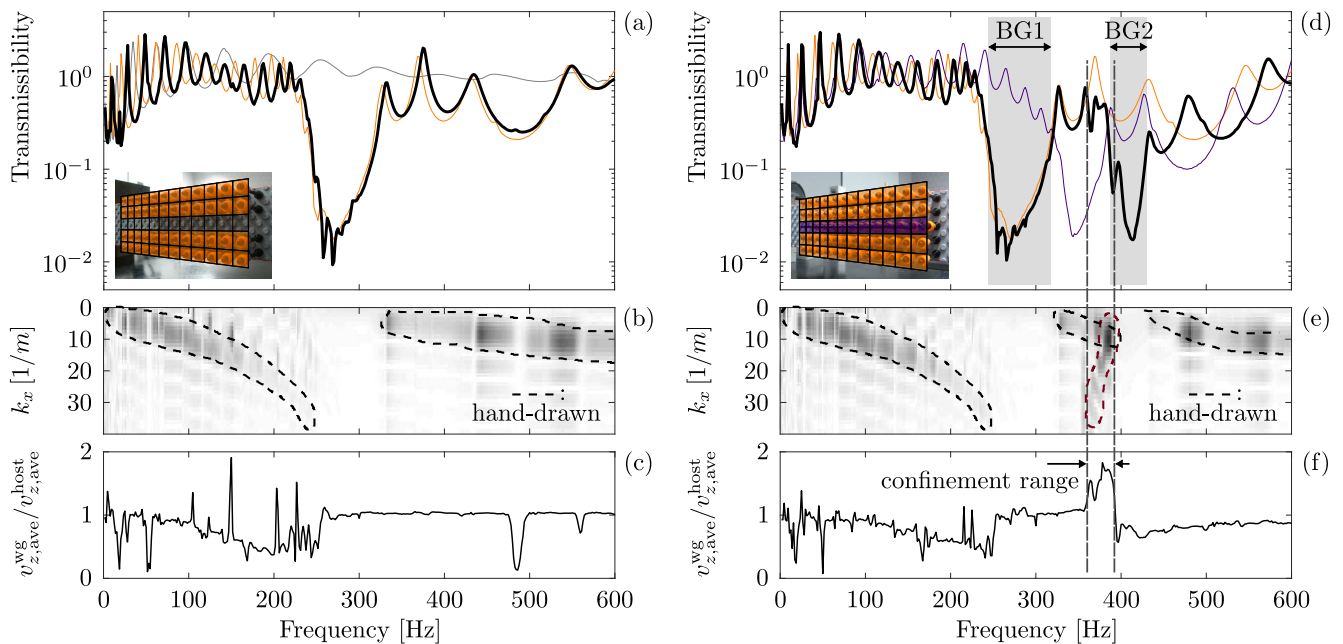


FIGURE 6: (a) Transmissibility (thick black line) of a configuration featuring an empty line of defects in a M1 host (thin gray line refers to pillar-free plate, orange line to homogeneous M1 population). (b) Dispersion relation for configuration (a) reconstructed from steady-state measurements along the waveguide. (c) Amplitude ratio between measurements inside the waveguide and inside the pillar-populated area. (d) Transmissibility of a subwavelength waveguide obtained by opening a line of M5 resonators in M1 host (thin colored lines refer to uniformly tuned M1 and M5 configurations). (e) Reconstructed dispersion relation for configuration (d). (f) Amplitude ratio plot for configuration (d).

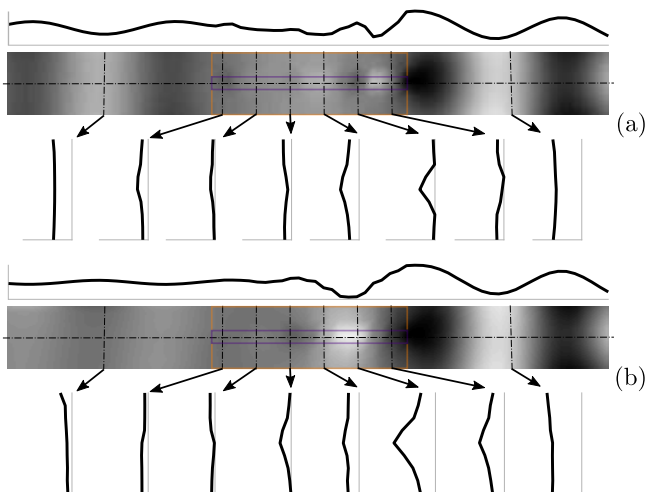


FIGURE 7: Subwavelength waveguiding obtained via a line of M5 resonators in M1 host. (a) Laser-acquired out-of-plane normalized velocity field at 366 Hz (color-coded lines mark regions occupied by the corresponding pillar type). The figure also includes one horizontal and several vertical sections of the measured response to better visualize the confinement within the waveguide path. (b) Same analysis for the 378 Hz case.

the absence of significant spikes in the neighborhood of the bandgap region confirms the absence of confinement.

The case of a subwavelength waveguide consisting of a line of (up-shifted) M5 resonators in a M1 host is shown

in Figs. 6d-f. The transmissibility plot in Fig. 6d features now two bandgaps (BG1 and BG2) separated by a transmission region. While the shape of the transmission plot is characteristic of subwavelength waveguiding conditions [7, 10], this result is peculiar in that the transmission region is not located inside, but rather right above the bandgap obtained with a uniform M1 population. Interestingly, here we observe a second bandgap which, despite possessing the same morphological characteristics of the M5 configuration, is “pushed-up” in frequency. These conditions, systematically observed over a large number of test cases (see *Supplementary Material*), seem to elude the rationale that has been successfully invoked in [7] to describe up-shifting mechanisms in acoustic media. The sources of this discrepancy may lie in the different coupling mechanisms available for the pillar resonators through the elastic substrate, compared to those provided by air in the acoustic case; a definitive assessment of these conjectures will require further investigations. From the dispersion plot of Fig. 6e, we recognize two branches inside the new transmission region between the two bandgaps. While the one circled by the black line is confined to the long-wavelength regime, the one highlighted in maroon extends over the entire Brillouin zone and features negative group velocity, which implies that low frequencies excite short wavelengths, and vice-versa. From the amplitude ratio plot of Fig. 6f, we can see that, at these frequencies, the response is indeed confined within the waveguide.

In Fig. 7 we show the velocity wavefields reconstructed

with the laser vibrometer for the configuration described in Fig. 6d at two frequencies (366 Hz and 378 Hz, both falling inside the confinement range highlighted Fig. 6f). For each frequency, the response is plotted as a color map of the steady-state velocity field (normalized by the maximum value recorded for that frequency). In contrast with the case of a conventional waveguide, we detect a signal with a defined wavelength structure established along the path of upshifted resonators and confined within its width, which suggests that both information and energy are partially transmitted along the waveguide. To better showcase the subwavelength transport and confinement, we enrich the description with a horizontal section of the response measured along a line running along the waveguide path, as well as with several vertical sections spanning the width of the strip perpendicularly to the waveguide. The spikes observed at the center of the vertical sections intersecting the waveguide confirm that the response localizes within the width of the waveguide. The confinement is especially accentuated at 378 Hz (Fig. 7b), for which the wavelength structure of the transmitted signal is also better defined. We can also appreciate that the wavelength of the confined signal increases with frequency in the transmission band, in accordance with the negative slope of the wave mode highlighted in maroon in Fig. 6e.

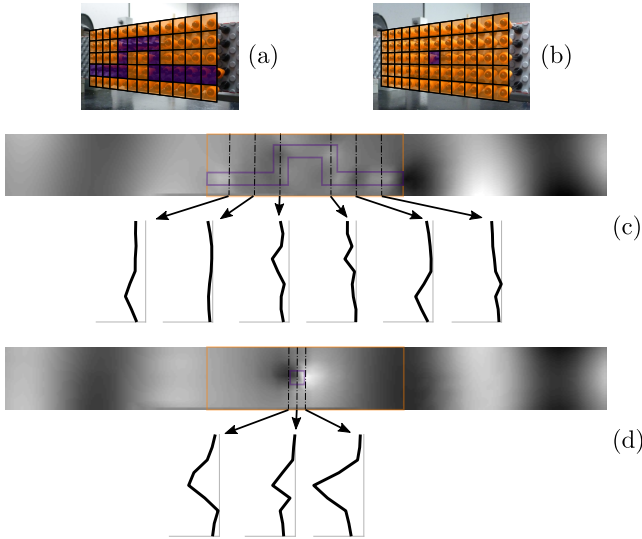


FIGURE 8: (a)  $\Omega$ -shaped waveguide (M1 host, M5 waveguide). (b) Single M5 defect in host of M1 resonators. (c) Out-of-plane normalized velocity field for configuration (a), at 364 Hz. (d) Velocity field for configuration (b), at 380 Hz.

To demonstrate the robustness of the subwavelength mechanism against changes in shape and to hint at the plethora of wave manipulation effects that could be implemented by playing with the design parameters, in Fig. 8 we report the results obtained for two other heterogeneous configurations that are simply obtained by tuning the resonators according to a different spatial pattern (note that these additional tests were obtained in a different experi-

mental session with slightly different setup details). The first example is an  $\Omega$ -shaped waveguide: the shifting peaks in the vertical sections in Fig. 8c show that the information is laterally confined and transmitted along the tortuous path of the waveguide. The second example is a subwavelength cavity obtained by upshifting a single resonating pillar: it is evident from the wavefield in Fig. 8d that the response localizes in the neighborhood of that resonator.

## Conclusions

In this article, we have demonstrated the versatility and technological potential of mechanical metamaterials featuring spatially disordered, heterogeneously-tuned resonators. We have realized and tested a tunable elastodynamic rainbow trap and we have shown that the interplay between heterogeneity and disorder results in a magnification of the filtering effects displayed by more conventional spatially-ordered rainbow material concepts. We have also provided a first body of experimental evidence of subwavelength localization of elastic waves, and commented on analogies and notable anomalies with respect to similar phenomena observed in acoustic media. Through the versatility of our tunable platform, we have been able to reconfigure the specimen to test a plethora of subwavelength waveguiding and confinement conditions.

## Materials and methods

The specimen is a strip cut out from a gray acrylonitrile butadiene styrene (ABS) baseplate (LEGO<sup>®</sup>, Item 10701) and features  $12 \times 5$  telescopic resonators arranged in a square lattice architecture. The strip is 5.7 cm wide and the distance between the clamped ends is approximately 46.3 cm. Each resonator is characterized by a rod (LEGO<sup>®</sup>, Elem. ID 395726) and a conical brick (LEGO<sup>®</sup>, Elem. ID 4518029) in prismatic contact. The conical brick can be slid up and down the rod to tune the resonator's natural frequency; the rod-brick contact is strong enough for the brick to hold its position throughout the tests. Note that the resonators are attached to the baseplate through frictional contact as well (anchoring the base of the rod to one of the protuberances—*studs*—of the baseplate). The standing wave excitation signals are transmitted to the structure through an electromechanical shaker (Brüel & Kjær Type 4810) and a stinger. The out of plane velocity time histories of points on the back-side of the plate belonging to a pre-determined grid are recorded via a 3D Scanning Laser Doppler Vibrometer (3D-SLDV, Polytec PSV-400-3D). The acquisition is performed in the frequency domain (the Fast Fourier Transform is performed automatically within the PSV acquisition system). To eliminate non-repeatable noisy features from the response, measurements are repeated 10 times and averaged at each measurement location. Additional details on the acquisition settings are reported in the *Supplementary Material*. The excitation is a pseudorandom waveform with maximum amplitude of 500 mV. The excitation signal is amplified using a Brüel & Kjær Type 2718 Power Amplifier, with gain set to 30 dB.

## Acknowledgements

S.G. and P.C. acknowledge the support of the National Science Foundation (grant CMMI-1266089). P.C. acknowledges the support of the University of Minnesota through the Doctoral Dissertation Fellowship. We thank Weiting Zhang and Nathan Bausman for their assistance and for helpful discussions, Mugurel Tuross for helping with the setup, Kai Sun of the University of Michigan, Vincent Tournat and Alejandro Cebrecos of the l'Université du Maine for fruitful discussions.

- 
- [1] Z. Liu, X. Zhang, Y. Mao, Y. Y. Zhu, Z. Yang, C. T. Chan, and P. Sheng. Locally resonant sonic materials. *Science*, 289(5485):1734–1736, 2000.
  - [2] H. Zhu and F. Semperlotti. Anomalous refraction of acoustic guided waves in solids with geometrically tapered metasurfaces. *Phys Rev Lett*, 117:034302, 2016.
  - [3] A.-C. Hladky-Hennion, J. O. Vasseur, G. Haw, C. Cronne, L. Haumesser, and A. N. Norris. Negative refraction of acoustic waves using a foam-like metallic structure. *Appl Phys Lett*, 102(14):144103, 2013.
  - [4] S. Zhang, C. Xia, and N. Fang. Broadband acoustic cloak for ultrasound waves. *Phys Rev Lett*, 106:024301, 2011.
  - [5] J. Zhu, J. Christensen, J. Jung, L. Martin-Moreno, X. Yin, L. Fok, X. Zhang, and F. J. Garcia-Vidal. A holey-structured metamaterial for acoustic deep-subwavelength imaging. *Nat Phys*, 7(1):52–55, 2011.
  - [6] K. L. Tsakmakidis, A. D. Boardman, and O. Hess. Trapped rainbow storage of light in metamaterials. *Nature*, 450(7168):397–401, 2007.
  - [7] F. Lemoult, N. Kaina, M. Fink, and G. Lerosey. Wave propagation control at the deep subwavelength scale in metamaterials. *Nat Phys*, 9(1):55–60, 2013.
  - [8] M. Addouche, M. A. Al-Lethawe, A. Elayouch, and A. Khelif. Subwavelength waveguiding of surface phonons in pillars-based phononic crystal. *AIP Adv*, 4(12):124303, 2014.
  - [9] Z. Gao, F. Gao, and B. Zhang. Guiding, bending, and splitting of coupled defect surface modes in a surface-wave photonic crystal. *Appl Phys Lett*, 108(4):041105, 2016.
  - [10] N. Kaina, A. Causier, Y. Bourlier, M. Fink, T. Berthelot, and G. Lerosey. Slow waves in locally resonant metamaterials line defect waveguides. *arXiv:1604.08117v1*, 2016.
  - [11] J. Zhu, Y. Chen, X. Zhu, F. J. Garcia-Vidal, X. Yin, W. Zhang, and X. Zhang. Acoustic rainbow trapping. *Sci Rep*, 3:1728, 2013.
  - [12] S. Krödel, N. Thomé, and C. Daraio. Wide band-gap seismic metastructures. *Extreme Mech Lett*, 4:111–117, 2015.
  - [13] D.-G. Zhao, Y. Li, and X.-F. Zhu. Broadband lamb wave trapping in cellular metamaterial plates with multiple local resonances. *Sci Rep*, 5:9376, 2015.
  - [14] D. Cardella, P. Celli, and S. Gonella. Manipulating waves by distilling frequencies: a tunable shunt-enabled rainbow trap. *Smart Mater Struct*, 25(8):085017, 2016.
  - [15] Z. Tian and L. Yu. Rainbow trapping of ultrasonic guided waves in chirped phononic crystal plates. *Sci Rep*, 7:40004, 2017.
  - [16] A. Colombi, V. Ageeva, R. J. Smith, A. Clare, R. Patel, M. Clark, D. Colquitt, P. Roux, S. Guenneau, and R. V. Craster. Enhanced sensing and conversion of ultrasonic rayleigh waves by elastic metasurfaces. *Sci. Rep.*, 7:6750, 2017.
  - [17] T.-T. Wu, Z.-G. Huang, T.-C. Tsai, and T.-C. Wu. Evidence of complete band gap and resonances in a plate with periodic stubbed surface. *Appl Phys Lett*, 93(11):111902, 2008.
  - [18] Y. Pennec, B. Djafari-Rouhani, H. Larabi, J. O. Vasseur, and A. C. Hladky-Hennion. Low-frequency gaps in a phononic crystal constituted of cylindrical dots deposited on a thin homogeneous plate. *Phys Rev B*, 78:104105, 2008.
  - [19] M. Oudich, M. Senesi, M. B. Assouar, M. Ruzenne, J.-H. Sun, B. Vincent, Z. Hou, and T.-T. Wu. Experimental evidence of locally resonant sonic band gap in two-dimensional phononic stubbed plates. *Phys Rev B*, 84:165136, 2011.
  - [20] M. Badreddine Assouar, Matteo Senesi, Mourad Oudich, Massimo Ruzzene, and Zhilin Hou. Broadband plate-type acoustic metamaterial for low-frequency sound attenuation. *Appl Phys Lett*, 101(17):173505, 2012.
  - [21] F. Casadei, T. Delpero, A. Bergamini, P. Ermanni, and M. Ruzzene. Piezoelectric resonator arrays for tunable acoustic waveguides and metamaterials. *J Appl Phys*, 112(6):064902, 2012.
  - [22] Y. Achaoui, V. Laude, S. Benchabane, and A. Khelif. Local resonances in phononic crystals and in random arrangements of pillars on a surface. *J Appl Phys*, 114(10):104503, 2013.
  - [23] M. Rupin, F. Lemoult, G. Lerosey, and P. Roux. Experimental demonstration of ordered and disordered multiresonant metamaterials for lamb waves. *Phys Rev Lett*, 112:234301, 2014.
  - [24] R. Pourabolghasem, A. Khelif, S. Mohammadi, A. Asghar Eftekhari, and A. Adibi. Physics of band-gap formation and its evolution in the pillar-based phononic crystal structures. *J Appl Phys*, 116(1):013514, 2014.
  - [25] P. Celli and S. Gonella. Manipulating waves with LEGO® bricks: A versatile experimental platform for metamaterial architectures. *Appl Phys Lett*, 107(8):081901, 2015.
  - [26] Z. Wu, R. L. Harne, and K. W. Wang. Exploring a modular adaptive metastructure concept inspired by muscles cross-bridge. *J Intel Mat Syst Struct*, 27(9):1189–1202, 2016.
  - [27] S. Lee, B. Kang, H. Keum, N. Ahmed, J. A. Rogers, P. M. Ferreira, S. Kim, and B. Min. Heterogeneously assembled metamaterials and metadevices via 3d modular transfer printing. *Sci Rep*, 6:27621, 2016.

- [28] G. Memoli, M. Caleap, M. Asakawa, D. R. Sahoo, B. W. Drinkwater, and S. Subramanian. Metamaterial bricks and quantization of meta-surfaces. *Nat Commun*, 8:14608, 2017.
- [29] C. Goffaux and J. P. Vigneron. Theoretical study of a tunable phononic band gap system. *Phys Rev B*, 64:075118, 2001.
- [30] V. Romero-García, C. Lagarrigue, J-P. Groby, O. Richoux, and V. Tournat. Tunable acoustic waveguides in periodic arrays made of rigid square-rod scatterers: theory and experimental realization. *J Phys D: Appl Phys*, 46(30):305108, 2013.
- [31] M. Thota, S. Li, and K. W. Wang. Lattice reconfiguration and phononic band-gap adaptation via origami folding. *Phys Rev B*, 95:064307, 2017.
- [32] O. R. Bilal and M. I. Hussein. Trampoline metamaterial: Local resonance enhancement by springboards. *Appl Phys Lett*, 103(11):111901, 2013.
- [33] E. Coffy, T. Lavergne, M. Addouche, S. Euphrasie, P. Vairac, and A. Khelif. Ultra-wide acoustic band gaps in pillar-based phononic crystal strips. *J Appl Phys*, 118(21):214902, 2015.
- [34] J. H. Oh, H. M. Seung, and Y. Y. Kim. Adjoining of negative stiffness and negative density bands in an elastic metamaterial. *Appl Phys Lett*, 108(9):093501, 2016.
- [35] O. Thorp, M. Ruzzene, and A. Baz. Attenuation and localization of wave propagation in rods with periodic shunted piezoelectric patches. *Smart Mater Struct*, 10(5):979, 2001.
- [36] R. Sainidou, N. Stefanou, and A. Modinos. Widening of phononic transmission gaps via anderson localization. *Phys Rev Lett*, 94:205503, 2005.
- [37] C. H. Hodges. Confinement of vibration by structural irregularity. *J Sound Vib*, 82(3):411–424, 1982.
- [38] J. A. Judge, B. H. Houston, D. M. Photiadis, and P. C. Herdic. Effects of disorder in one- and two-dimensional micromechanical resonator arrays for filtering. *J Sound Vib*, 290(3-5):1119–1140, 2006.
- [39] Hefei Hu, A. Strybulevych, J. H. Page, S. E. Skipetrov, and B. A. van Tiggelen. Localization of ultrasound in a three-dimensional elastic network. *Nat Phys*, 4:945–948, 2008.
- [40] M. Oudich, M. B. Assouar, and Z. Hou. Propagation of acoustic waves and waveguiding in a two-dimensional locally resonant phononic crystal plate. *Appl Phys Lett*, 97(19):193503, 2010.
- [41] W. Jiang, D. Feng, D. Xu, B. Xiong, and Y. Wang. Experimental investigation of energy localization in line-defect resonator based on silicon locally resonant phononic crystal. *Appl Phys Lett*, 109(16):161102, 2016.
- [42] M. Addouche, M. A. Al-Lethawe, A. Elayouch, and A. Khelif. Subwavelength waveguiding of surface phonons in pillars-based phononic crystal. *AIP Adv*, 4(12):124303, 2014.

## Supplemental material (SM)

### Additional details on the experimental setup

In addition to the information reported in the *Materials and Methods* section, we here add details on the settings we selected for the 3D-SLDV acquisition. As far as the vibrometer channel is concerned, we select a 5 V range and DC coupling. We acquire in the 0–5 kHz frequency range, and we concentrate on the 0–600 Hz band when postprocessing the data. The sampling frequency is  $f_s = 12.8$  kHz and the number of FFT lines is 3200, resulting in a frequency resolution of 1.5625 Hz. The selected velocity decoder is the digital VD-08-10 mm/s/V, that allows acquisitions up to 20 kHz.

Throughout this work, we used two different setups, featuring the same specimen but slightly different boundary conditions (due to the fact that it is nearly impossible to clamp the specimen exactly the same way twice): the first setup is used throughout the bandgap analysis and for most of the subwavelength waveguiding experiments, while the second one is used for the  $\Omega$ -shaped waveguide and for the point defect experiments. Inevitably, the two setups are characterized by a slightly different response; while the bandgap onset associated with a specific type of resonator is unaffected by changes in the boundary conditions, other characteristics such as the bandgap profile and the resonant peaks of the structure will be altered. The transmissibilities of the specimen for both setups, corresponding to several uniform resonator configurations, are shown in Fig. S1. Fig. S1a represents the response of the first setup, the one used throughout the bandgap analysis (this figure coincides with Fig. 3 of the main article). The colored lines correspond to different configurations, as shown in the corresponding inserts. It is interesting to see how the dips in the transmissibilities are only due to the presence of the bricks, as highlighted by the almost-flat response of the specimen without bricks (gray line). We can also appreciate how the resonators are tuned at adjacent frequencies, as displayed by the fact that their bandgaps are overlapping. Similar considerations can be made for the second setup, the one used for the wave localization experiments, whose response is shown in Fig. S1b.

Our specimens are extremely flexible and are made of a polymeric material. To rule out nonlinearities from our explanations, we tried to understand whether our specimens presented any signature of nonlinearity in their response. In order to address this issue, we compared the responses of the same architecture featuring only M1 resonators to excitations at different amplitudes. The transmissibility plots for three loading amplitudes (0.1 V, 0.5 V—the amplitude used for all experiments throughout this article—and 1.0 V) are superimposed in Fig. S2. We can see that the only difference between the 0.1 V case and the 0.5 V case is represented by the morphology of the bandgap—with the 0.1 V case being characterized by a jagged “bottom”. With re-

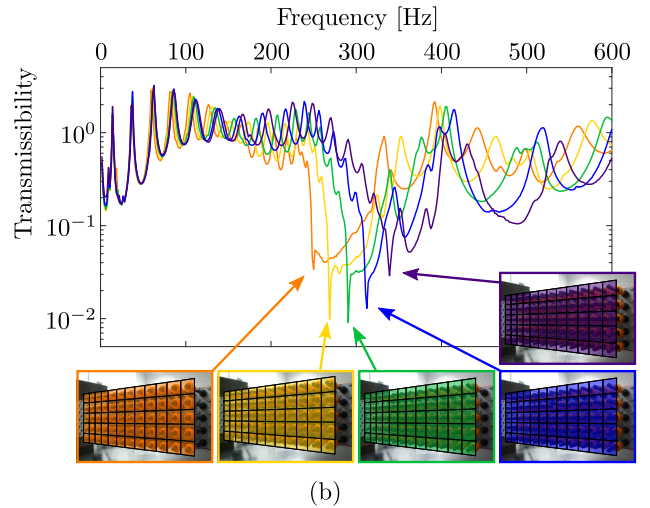
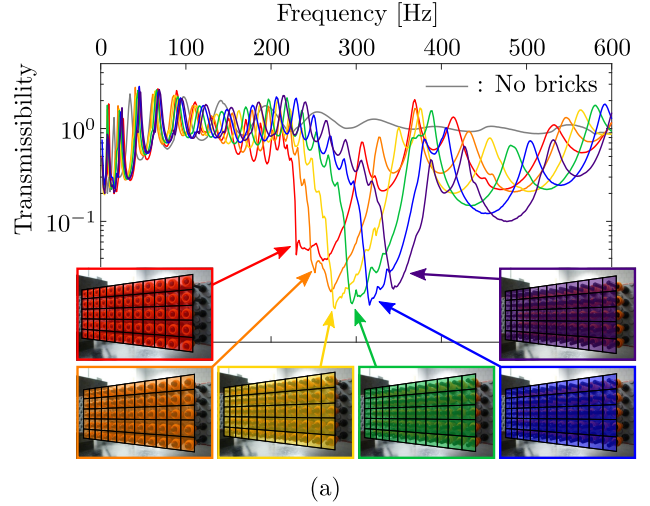


FIGURE S1: (a), (b) Comparison between the transmissibilities of configurations featuring uniform arrangements of  $5 \times 12$  bricks. The two sets of results differ slightly in terms of boundary conditions of the specimen.

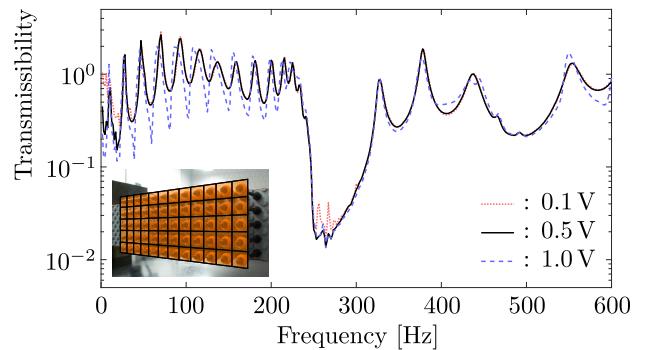


FIGURE S2: Response of a uniform M1 architecture to three different loading amplitudes.

spect to the other two cases, the high amplitude (1.0 V) one is characterized by a different response both before and after the bandgap. We believe this amplitude-dependent

behavior to be indeed due to a mix of material and geometric nonlinearities that are triggered when the load is larger than a certain threshold. However, we exclude that nonlinearities affect our observations on bandgap widening, due to the fact that the amplitude of excitation does not significantly affect the extent of the bandgap, whose sharp onset and sloping end are unchanged.

### More on broadband wave attenuation

In this section, we report additional results related to the attenuation capabilities of architectures featuring functionally-graded and disordered spatial arrangements. In the article, we reported on various architectures displaying 10 resonators of each of the following types: T, M1, M2, M3, M4, M5. In Fig. S3, we show that similar considerations can be made for architectures comprising 15 M1, 15 M2, 15 M3 and 15 M4 resonators. We can see that bandgaps for the functionally graded architectures, shown in Figs. S3a-b, span two of the reference bandgaps (yellow and green) and present a similar morphology (sharp onset and sloping end). On the other hand, the bandgaps of configurations featuring disordered brick arrangements are wider than their graded counterparts, spanning three or four individual bandgaps as shown in Figs. S3c-e, and also present different morphological characteristics (they have a “jagged” profile, while also being less deep).

In Fig. S4, we show the response of architectures comprising 30 M1 and 30 M2 resonators. As we decrease the degree of heterogeneity among resonator characteristics, we can see that the results for functionally-graded and disordered architectures do not differ much. Even though it is challenging to make qualitative comments about bandgap width, we are able to see that the bandgaps in Figs.6d-f have a more regular morphology than those in Figs. S4c-e.

### More on subwavelength localization

In this section, we show additional results in terms of waveguiding and confinement that complement those reported in the main article. First of all, we compare the reconstructed band diagram for the case of a straight M5 waveguide in a M1 host (Fig. S5d) to the band diagrams obtained for a bare baseplate (Fig. S5a), for a uniform M1 (Fig. S5b) and for a uniform M5 architecture (Fig. S5c). We can see that, with respect to the bare baseplate case, the introduction of a uniform population of M1 resonators causes the splitting of the flexural wave propagation mode and the generation of a hybridization bandgap. As we tune the resonators to the M5 configuration, as expected, we cause the bandgap to shift towards higher frequencies. Introducing a M5 straight waveguide within a M1 architecture, as discussed in the main article, causes the arising of two bandgaps and of a negative group velocity mode. The latter mode is correlated to the manifestation of subwavelength wave confinement.

We now analyze other waveguide architectures characterized by a M1 host. The results for an empty waveguide,

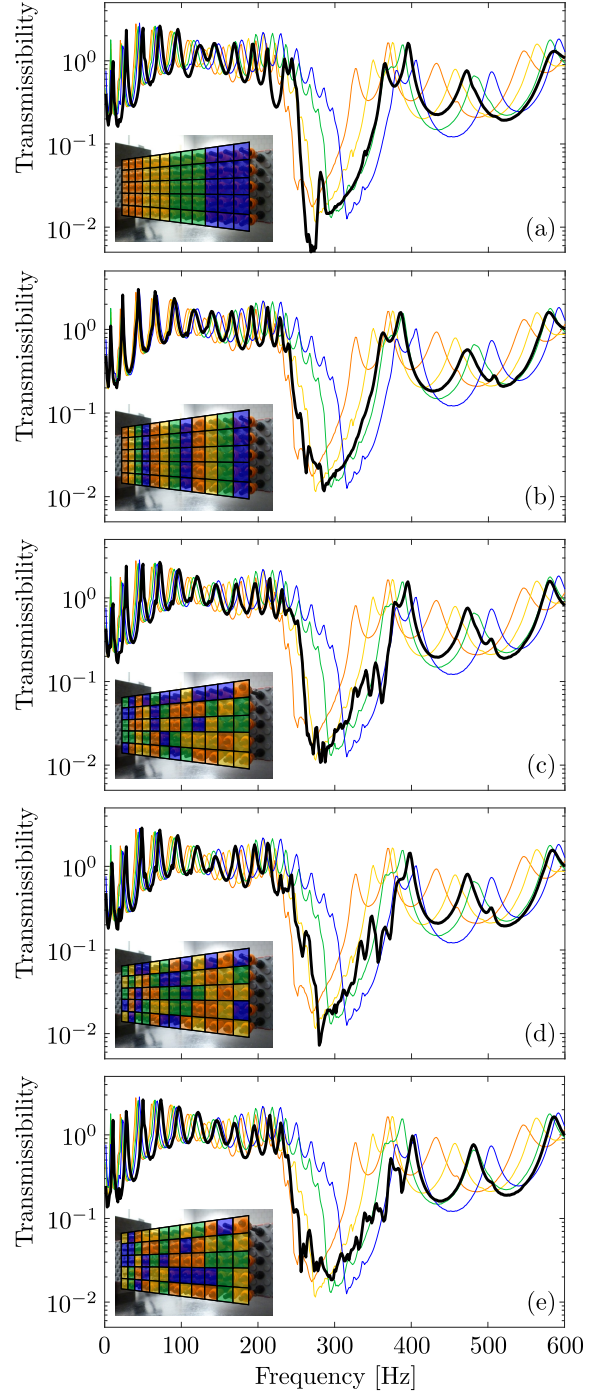


FIGURE S3: Influence of the spatial arrangement of heterogeneously tuned resonators on wave attenuation. In all cases, 10/60 resonators are programmed to the brick configurations M1, M2, M3 and M4. (a), (b) Transmissibilities for functionally graded and (c), (d), (e) spatially randomized configurations, marked by thick black lines; thin color-coded lines refer to uniformly tuned monochromatic configurations (see color coding in Fig. 1b).

also shown in the main article, are reported in Figs. S6a-b. Fig. S6a highlights how the introduction of an empty waveguide does not produce significant effects from a transmis-

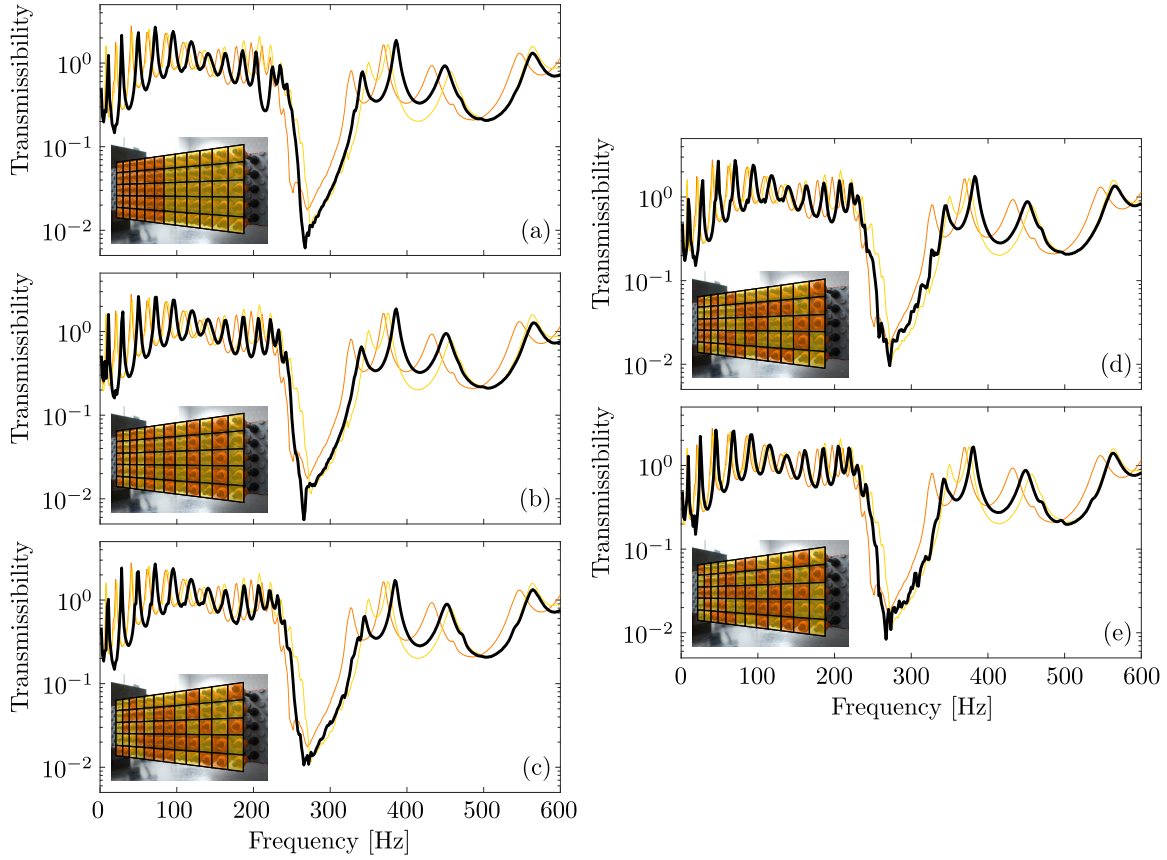


FIGURE S4: Influence of the spatial arrangement of heterogeneously tuned resonators on wave attenuation. In all cases, 30/60 resonators are programmed to the brick configurations M1, M2. (a), (b) Transmissibilities for functionally graded and (c), (d), (e) spatially randomized configurations, marked by thick black lines; thin color-coded lines refer to uniformly tuned monochromatic configurations (see color coding in Fig. 1b).

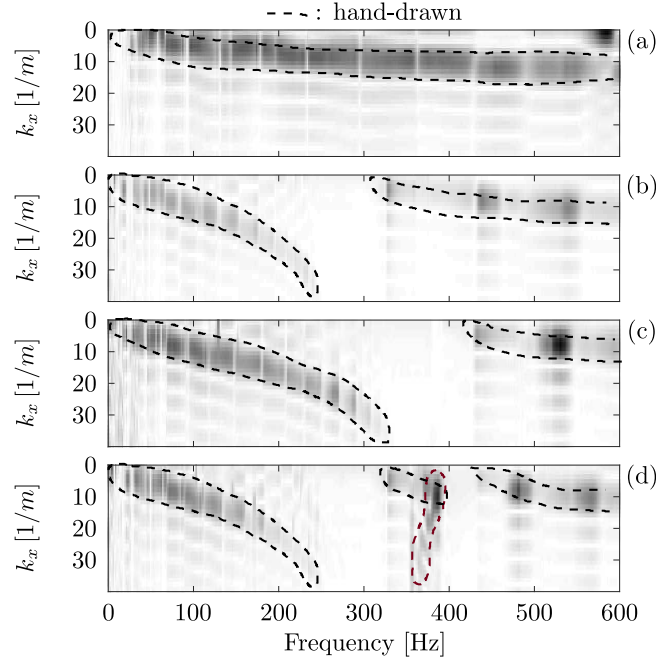


FIGURE S5: Reconstructed dispersion relation for a line of measurement points within the waveguide. (a) Bare baseplate. (b) Uniform M1 architecture. (c) Uniform M5 architecture. (d) M5-in-M1 waveguide case.

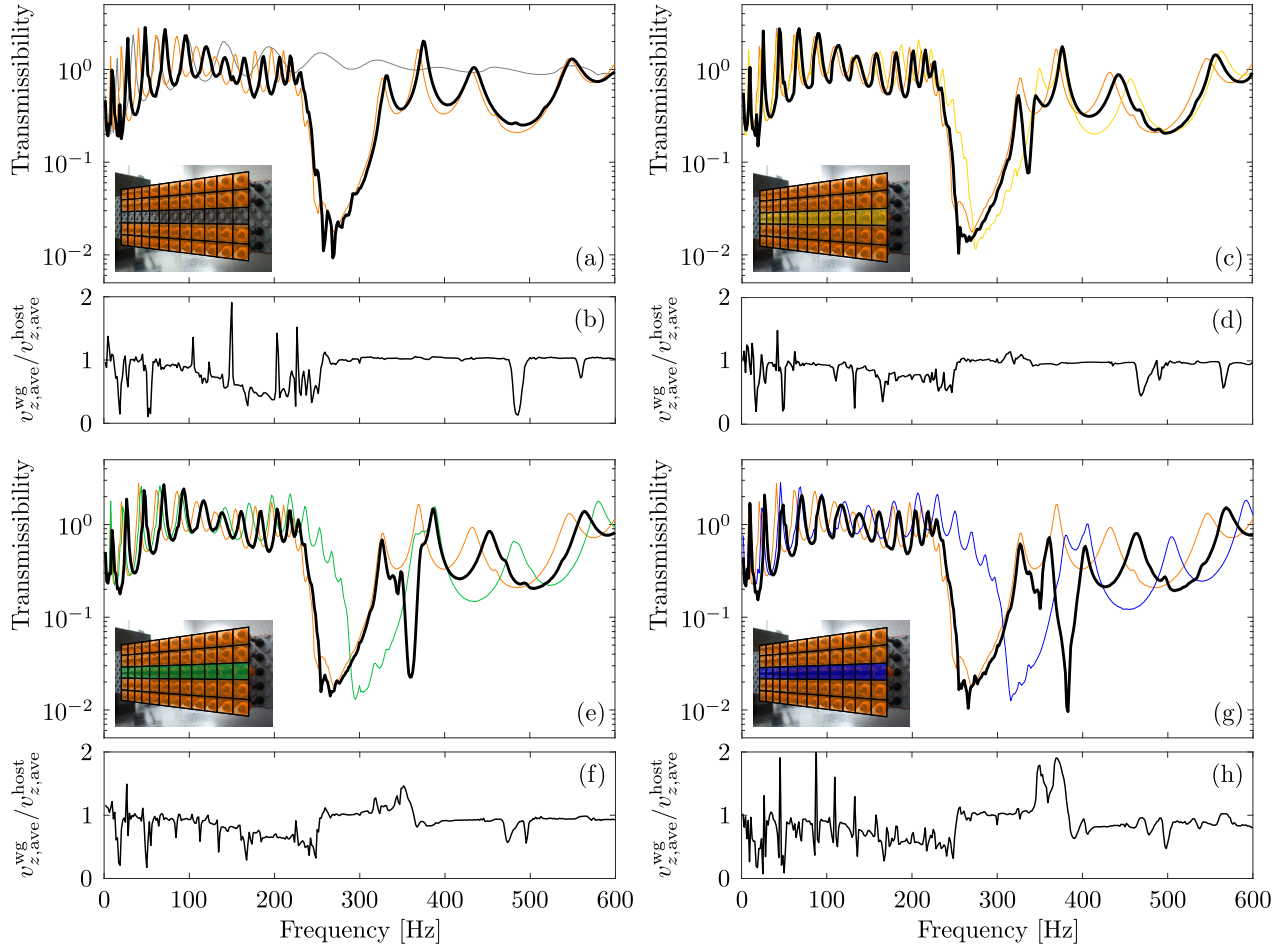


FIGURE S6: (a), (c), (e), (g) Straight waveguides (featuring a M1 host and empty, M2, M3, M4 lines of defects, respectively). (b), (d), (f), (h) Amplitude ratios between measurements at points of the plate inside the waveguide and points in the brick-populated area, for the configurations in (a) and (c), (e), (g), respectively.

sibility standpoint. This is also visible from the amplitude ratio plot in Fig. S6b, which does not present any interesting feature in the neighborhood of the bandgap. The presence of M2 resonators within the path of defects, as shown in Figs. S6c-d is still not enough to produce localization effects. Things change when we place M3 resonators within the waveguide, as shown in Figs. S6e-f. These up-shifted resonators clearly impact the transmissibility plot, where we record the appearance of a transmission region following the M1 bandgap and followed by a second thin gap, which extends up to the end of the M3 gap. Note that the structure seen in this transmissibility plot is analogous to that observed for the M5-in-M1 waveguide. In the M3 case, however, we clearly see that the waveguiding behavior is weaker than the one observed in Figs. 6d-f. Similar considerations apply to the M4-in-M1 waveguide, whose response (shown in Figs. S6g-h) is characterized by a stronger waveguiding, almost as pronounced as that of the M5-in-M1 case. In light of these results, we can conclude that not all up-shifted resonators produce confinement effects. As the resonant frequency of the up-shifted resonators grows larger, the confinement increases in inten-

sity (note that we did not consider resonators with resonant frequencies larger than that of M5). We can also conclude that confinement effects are always accompanied by a peculiar transmissibility plot featuring two bandgaps (the one of the host medium and a “pushed-up” one) and a transmission region in between; localization only occurs within the sub-region of this transmission region that corresponds to a negative group velocity mode as the one highlighted in maroon in Fig. S5d.